On Gravitational Binding Energy Evaluation

Nicolas Poupart[1]

[1]Independent Researcher, Quebec, Canada
[*]Corresponding author. E-mail: nicolas.poupart@yahoo.fr

Abstract. We develop a hierarchical formulation for evaluating gravitational binding energy from the internal organization of matter, volume conservation, and mass–energy equivalence. Rather than relying only on pairwise interaction terms defined relative to infinity, the proposed estimator assigns an intrinsic energy scale to compact configurations of matter. We then test whether the corresponding mass-equivalent contribution can reproduce the effective dark mass inferred in galaxies.

We test this formulation using SPARC rotation-curve data together with independent GALEX and SDSS photometric observations. Stellar population mixtures are reconstructed from dynamical information alone, without using photometric data as input, and are then used to predict integrated galaxy colors. The resulting colors show significant correlations with observations, indicating that the reconstructed populations encode non-trivial information about stellar structure.

A systematic exploration of the estimator reveals structured regions of high-quality solutions in parameter space. In particular, the results favor a hierarchical recursive interpretation in which class-level binding energies are preserved, while the binding energy associated with the global aggregation of heterogeneous stellar classes may contribute with an effective virial factor. The dynamical reconstruction varies only weakly across a broad range of parameters, whereas the photometric constraints provide greater discrimination between candidate forms.

These results suggest that gravitational binding energy provides a physically motivated contribution to the effective dark mass inferred in galaxies, while also explaining why dynamical information can encode stellar population structure.

Keywords. Gravitational binding energy—Galaxy dynamics—Rotation curves—Dark matter—Stellar populations—Galaxy photometry—Ultraviolet observations

1. Introduction

The origin of the dark mass component inferred from galactic dynamics remains one of the central open questions in astrophysics Courteau *et al*. (2014). Its presence is robustly established through multiple independent observations, including rotation curves and dynamical modeling (Rubin *et al*., 1980; Persic *et al*., 1996), as well as gravitational lensing measurements Clowe *et al*. (2006); Bartelmann (2010). However, its physical nature remains unknown.

At the same time, gravitational theory, both Newtonian and relativistic, has demonstrated remarkable accuracy across a wide range of scales. This raises the possibility that the observed discrepancy can be accounted for without invoking exotic matter or modified gravity, but by recognizing that gravitational potential energy is not straightforward to define and evaluate as an intrinsic contribution to the effective mass budget of astrophysical systems.

In standard formulations, gravitational potential energy is defined relative to an arbitrary reference level, typically taken at infinity. As a result, the expression $E = -GmM/d$ is well suited for describing reversible orbital dynamics, but it does not directly provide an intrinsic energy associated with the formation or internal organization of an extended many-body system.

More generally, the notion of potential energy becomes ambiguous when applied to complex self-gravitating systems. It quantifies the work required to separate constituents to infinity, rather than the energy associated with assembling matter into a bound configuration. Related ambiguities have long been recognized in classical mass renormalization Brillouin (1965) and in geometrical definitions of mass in general relativity Hawking (1968); Misner & Sharp (1964); Hayward (1996).

In this work, we define gravitational binding energy as an intrinsic energy associated with the assembly and internal organization of matter. The construction com-

pares distributed configurations to compact reference states while conserving mass and the intrinsic volumes of the constituents. This removes arbitrary reference levels and provides a reproducible evaluation of gravitational energy in heterogeneous systems.

This formulation naturally leads to a two-term structure. The first term represents the binding contribution of homogeneous stellar population classes, while the second describes the global heterogeneous aggregate. The recursive interpretation favors retaining the class-level contribution with its natural compact-sphere normalization, whereas the virial interpretation of the heterogeneous global aggregate motivates a reduction of the global contribution by a factor close to one half.

The empirical relevance of this formulation is tested using SPARC rotation-curve data together with independent GALEX and SDSS photometry. Stellar population mixtures are reconstructed from dynamical information alone, without using photometric data as input, and are then used to predict integrated galaxy colors. This provides a stringent test of whether the proposed binding-energy estimator encodes information not only about the effective dark mass inferred from dynamics, but also about the underlying stellar population structure.

The formalism developed here therefore provides a framework for investigating whether gravitational binding energy, evaluated hierarchically, can contribute to the effective mass budget of galaxies and link galactic dynamics to stellar population properties.

1.1 *Useful gravitational potential energy*

If we consider the Newtonian gravitational force equation, $F = GmM/d^2$, we obtain—by integrating from d to infinity—the potential energy formula $E_p = -GmM/d$. While this formulation yields negative potential energy which can be used for calculating the motion of celestial bodies, it is unsuitable for evaluating the total physical potential energy of a system.

To determine a physically meaningful energy scale, rather than a reference-dependent potential value, one must compute the energy difference between two states of the system—analogous to lifting a mass m from position d by a height h. In such a case:

$$\Delta E_p = E_p(d+h) - E_p(d) = \frac{GmMh}{d^2 + dh} \tag{1}$$

This expression represents the usable form of gravitational potential energy. The concept of absolute negative energy E_p is not directly interpretable in physical terms.

However, this formulation becomes impractical for systems involving two celestial bodies (e.g., planets, stars, or galaxies), because the initial reference distance d is undefined or ambiguous. To resolve this, we compute the energy difference between a compact state—a single solid spherical mass $M_t = m + M$—and a configuration of two distinct spherical bodies, m and M, separated by a distance d.

Let the two bodies have radii r and R, and volumes $v = 4\pi r^3/3$ and $V = 4\pi R^3/3$, with corresponding densities m/v and M/V. The total volume of the single solid sphere is $V_t = V + v = 4\pi(R^3 + r^3)/3$, and its radius $R_t = (R^3 + r^3)^{1/3}$. Assuming equal volumetric densities, $m/v = M/V$, that of the single compact ball will be identical: $m/v = M/V = M_t/V_t$; if not, it assumes an average density weighted by the contributions of m and M.

The gravitational potential energy of a homogeneous solid sphere is given by:

$$E_p = -\frac{3GM^2}{5R} \tag{2}$$

The gravitational binding energy of the system can be evaluated by comparing the initial state (a single compact mass) and the final state (two separated masses), the compact configuration being uniquely defined by mass conservation and volume conservation, ensuring that no additional physical interactions are introduced beyond gravity. The difference between these two states is then given by:

$$E_i = -\frac{3GM_t^2}{5R_t} \tag{3}$$

$$E_f = -\frac{3GM^2}{5R} - \frac{3Gm^2}{5r} - \frac{GMm}{d} \tag{4}$$

$$\Delta E_p = E_f - E_i = \left(-\frac{3GM^2}{5R} - \frac{3Gm^2}{5r} - \frac{GMm}{d}\right) + \frac{3GM_t^2}{5R_t} \tag{5}$$

This expression quantifies the energy change from a compact configuration to a system of two separated masses. It represents a redistribution of matter that preserves the original component densities, thereby ensuring that the transformation involves only gravitational forces.

1.2 *Mass-equivalent gravitational binding energy*

Gravitational potential energy is central to astrophysical dynamics, but its mass-equivalent contribution is usually assumed to be too small to account for the dark mass inferred in galaxies. The hierarchical formulation developed here challenges this assumption, since the

corresponding gravitational binding-energy scale can reach the galactic dark-mass regime.

A natural way to assess the physical relevance of this energy is to express it through the mass–energy equivalence relation $E = mc^2$. In this framework, any form of energy can be associated with an effective mass contribution, providing a direct comparison scale with baryonic mass.

More generally, it has long been recognized that gravitational energy contributes to the effective mass of a system and to the curvature of spacetime. This idea appears in classical considerations of mass renormalization Brillouin (1965) and is formalized in general relativity through quasi-local mass definitions such as the Hawking mass Hawking (1968) and related constructions in spherically symmetric spacetimes Misner & Sharp (1964); Hayward (1996). Together, these results support treating gravitational energy as part of the effective mass budget of self-gravitating systems.

In this context, gravitational binding energy may be interpreted as a physically meaningful component of the total mass–energy budget. When expressed via $E = mc^2$, it defines an effective mass scale that can be directly compared to observed mass components.

This perspective is also consistent with previous investigations suggesting that gravitational energy may contribute to an effective mass component in galactic systems Poupart (2014, 2025) and with numerical studies of gravitational self-interaction effects Deur *et al.* (2020); Deur (2021, 2022).

Finally, since the equivalence of inertial and gravitational mass has never been empirically violated MICROSCOPE Collaboration (2022), it is consistent, within current experimental limits, to treat gravitational binding energy as fully equivalent to its mass representation.

This effective mass interpretation is closely related to the notion of intrinsic energy of a system. In general, the energy stored within a bound configuration represents the amount of energy that can be released through a transformation of the system, and therefore converted into work or radiation.

In astrophysical contexts, such energy release is primarily associated with dynamical processes involving the restructuring of matter, most notably during collisions and mergers of gravitationally bound systems. These events provide a natural mechanism through which gravitational binding energy can be liberated and redistributed in the form of kinetic energy, heat, or electromagnetic radiation.

This perspective reinforces the interpretation of gravitational binding energy as a physically meaningful and measurable quantity, directly connected to observable energetic processes in the Universe.

1.3 *The binding energy of celestial bodies*

Table 1 contains the standard values for the celestial bodies under consideration, except for the radii for the globular cluster M80 and a representative galaxy. We modeled the initial state as a solid sphere of mass $M+m$, assuming solar density. The final state is the Sun at distance d of a mass M of solar density. For the Sun-M80 pair, the values used are $R = 5.534217 \cdot 10^{10}$, $R_t = 5.534221 \cdot 10^{10}$ and for the Sun-galaxy pair, the values used are $R = 2.03985712710655 \cdot 10^{12}$ and $R_t = 2.03985712713359 \cdot 10^{12}$. The rationale behind this construction will be addressed in a subsequent section. In either case, the radius is calculated using the relation $R_t = (R^3 + r^3)^{1/3}$.

Table 1. Physical parameters for celestial body pairs

System	m (kg)	M (kg)	r (m)
Moon+Earth	$7.35 \cdot 10^{22}$	$5.97 \cdot 10^{24}$	$1.74 \cdot 10^{6}$
Earth+Sun	$5.97 \cdot 10^{24}$	$1.99 \cdot 10^{30}$	$6.38 \cdot 10^{6}$
Jupiter+Sun	$1.90 \cdot 10^{27}$	$1.99 \cdot 10^{30}$	$6.99 \cdot 10^{7}$
Sun+M80	$1.99 \cdot 10^{30}$	$9.99 \cdot 10^{35}$	$6.96 \cdot 10^{8}$
Sun+Galaxy	$1.99 \cdot 10^{30}$	$5.00 \cdot 10^{40}$	$6.96 \cdot 10^{8}$

System	R (m)	d (m)	R_t (m)
Moon+Earth	$6.38 \cdot 10^{6}$	$3.8 \cdot 10^{8}$	$6.42 \cdot 10^{6}$
Earth+Sun	$6.96 \cdot 10^{8}$	$1.5 \cdot 10^{11}$	$6.96 \cdot 10^{8}$
Jupiter+Sun	$6.96 \cdot 10^{8}$	$7.8 \cdot 10^{11}$	$6.97 \cdot 10^{8}$
Sun+M80	$5.53 \cdot 10^{10}$	$4.5 \cdot 10^{17}$	$5.53 \cdot 10^{10}$
Sun+Galaxy	$2.04 \cdot 10^{12}$	$5.0 \cdot 10^{20}$	$2.04 \cdot 10^{12}$

Table 2 presents the gravitational potential energy differences between current physical configurations and their hypothetical fusion into a single mass. For scale, the complete conversion of 1 kg of mass into energy corresponds to 8.99×10^{16} J or about 21.5 megatons of TNT. This is of the same order as the largest thermonuclear tests ever performed, and would correspond, in an ideal deuterium–tritium fusion process, to approximately 105 kg of deuterium and 158 kg of tritium.

Based on this equivalence, the merger of the Moon with the Earth would release energy equivalent to approximately 40 trillion hydrogen bombs. This binding energy corresponds to a mass of about 40 billion metric tons—a value that is far from negligible.

If we consider the energy released by merging the Earth into the Sun, the resulting energy would correspond to over 14 million billion metric tons. However, this value is still less than the mass the Sun loses each hour due to nuclear fusion. Depending on its spatial distribution, this energy-equivalent mass could, in principle, be measurable.

Table 2. Gravitational potential energy differences and mass equivalents

System	E_i (J)	E_f (J)
Moon+Earth	$-2.2795 \cdot 10^{32}$	$-2.2413 \cdot 10^{32}$
Earth+Sun	$-2.2751 \cdot 10^{41}$	$-2.2751 \cdot 10^{41}$
Jupiter+Sun	$-2.2787 \cdot 10^{41}$	$-2.2751 \cdot 10^{41}$
Sun+M80	$-7.2141 \cdot 10^{50}$	$-7.2141 \cdot 10^{50}$
Sun+Galaxy	$-4.9079 \cdot 10^{58}$	$-4.9079 \cdot 10^{58}$

System	ΔE_p (J)	ΔE_p (kg)	$\Delta E_p/m$
Moon+Earth	$3.8176 \cdot 10^{30}$	$4.2477 \cdot 10^{13}$	$5.8 \cdot 10^{-10}$
Earth+Sun	$1.3024 \cdot 10^{36}$	$1.4491 \cdot 10^{19}$	$2.4 \cdot 10^{-6}$
Jupiter+Sun	$3.5519 \cdot 10^{38}$	$3.9520 \cdot 10^{21}$	$2.1 \cdot 10^{-6}$
Sun+M80	$2.3949 \cdot 10^{45}$	$2.6647 \cdot 10^{28}$	$1.34 \cdot 10^{-2}$
Sun+Galaxy	$3.2540 \cdot 10^{48}$	$3.6206 \cdot 10^{31}$	18.2

If we examine the ratio $(\Delta E_p/c^2)/m$, representing the binding-energy mass equivalent relative to the mass of the smaller body, we find that it is negligible in most cases—except at the galactic scale, where it approaches the order of magnitude of the observed dark mass ratio.

This shows that the binding contribution behaves as an endothermic binding energy, in a sense analogous to nuclear binding near the iron peak. For example, splitting an ^{56}Fe nucleus into two ^{28}Si nuclei requires energy, since the total mass of the two fragments is larger than the mass of the original nucleus. The bound state therefore has a lower mass than the separated products.

There is, however, an important difference between nuclear and gravitational binding. In the nuclear case, mass remains strictly separable once the final nuclei are specified. The mass of n isolated ^{28}Si nuclei is simply $n\,M(^{28}\mathrm{Si})$. Gravitational binding energy does not have this property. The mass-equivalent contribution associated with gravitational binding cannot be uniquely assigned to individual particles or separated into independent local masses. It is a global contribution associated with the interacting configuration.

This feature is dictated by the structure of general relativity. Unlike matter energy, gravitational field energy cannot be represented by a unique local density that is independent of coordinates and observers. It is instead characterized by global or quasi-local mass definitions, which depend on the gravitational system being probed Hawking (1968); Misner & Sharp (1964); Hayward (1996).

In this operational sense, the mass-equivalent contribution of gravitational binding is not separable into individual particle masses, but belongs to the interacting gravitational configuration.

Thus, an observer probing an isolated body of mass m measures only that mass, whereas an observer probing a system of n interacting bodies of masses m_i measures an effective gravitational source of the form:

$$\sum_i m_i + \frac{E_B}{c^2}$$

where E_B denotes the binding-energy contribution of the configuration. Here, the term "observer" should be understood operationally, as a test body responding to the gravitational field generated by either a single mass or by a composite interacting system.

In the galactic case, this means that a star located at radius r responds not only to the baryonic mass enclosed within that radius, but also to the effective mass associated with the gravitational binding energy of the enclosed matter.

2. The binding energy of celestial systems

The first observation is that the interaction term $-GmM/d$ in ΔE_p becomes negligible compared to internal self-energy terms in gravitational systems characterized by large scale separation. This result is intuitive from a physical standpoint, altering the distance between two celestial bodies, such as the Earth and the Moon, leads to minimal changes in gravitational energy compared to the energy released by their hypothetical fusion. This approximation holds across all celestial systems.

To quantify this, we compare the interaction energy to the dominant internal term:

$$\frac{GMm/d}{GM^2/R} = \frac{m}{M} \cdot \frac{R}{d} \tag{6}$$

For elementary astrophysical bodies such as planets and stars, this ratio is typically very small due to both mass hierarchy and spatial separation:

$$\frac{m}{M} \ll 1 \quad \text{and} \quad \frac{R}{d} \ll 1 \tag{7}$$

This property is not restricted to a particular scale but reflects a general feature of gravitational structure formation. Bound objects occupy a negligible volume compared to the space that separates them.

This can be verified explicitly at galactic scale. Even if all stars in a galaxy are hypothetically merged into a single compact object under volume conservation, the resulting radius scales as $N^{1/3}$ and remains extremely small compared to interstellar distances. For a Milky Way–type galaxy, one finds:

$$\frac{R}{d} \sim 10^{-4} \tag{8}$$

In a hierarchical construction where composite bodies are formed through successive mergers conserving density, both the effective radius and the characteristic separation scale as $N^{1/3}$. Therefore, the ratio R/d remains small at every level of aggregation.

It is important to emphasize that the effective binding-energy contribution used here is not obtained by assigning a positive mass to the conventional pairwise potential term $-GmM/d$. On the contrary, this term becomes negligible in the hierarchical astrophysical regime considered here. The dominant contribution arises from the compact-reference self-energy terms proportional to M^2/R, which compare configurations of different internal organization under mass and volume conservation.

Accordingly, the interaction term $-GmM/d$ can be neglected to leading order in the energy balance. The energy expression thus simplifies to:

$$\Delta E_p = \frac{3G}{5}\left(\frac{M_t^2}{R_t} - \alpha_M \frac{M^2}{R} - \alpha_m \frac{m^2}{r}\right) \tag{9}$$

where α_M and α_m encode the internal mass distribution of the bodies. For homogeneous solid spheres, $\alpha = 1$, but more generally $\alpha \sim O(1)$ depends on the density profile.

This implies that the spatial arrangement of bodies relative to one another is subdominant for calculating total gravitational binding energy. In this sense, the energy of the system must be treated as a global quantity, not reducible to a simple sum of pairwise interactions Landau & Lifshitz (1976). If we consider a system of n masses m_i with radii r_i, merged sequentially, we obtain the following expressions:

$$M_i = \sum_{j\le i} m_j, \quad R_i = \left(R_{i-1}^3 + r_i^3\right)^{1/3} \tag{10}$$

$$\Delta E_i = \frac{3G}{5}\left(\frac{M_i^2}{R_i} - \frac{M_{i-1}^2}{R_{i-1}} - \alpha_i \frac{m_i^2}{r_i}\right), \quad \Delta E_p = \sum_{i\le n} \Delta E_i \tag{11}$$

The relation $R_i^3 = R_{i-1}^3 + r_i^3$ follows from volume conservation. Individual stars may exhibit complex internal structures, which are encoded in the coefficients α_i, but these do not affect the final form of the total energy in the large-n limit.

Indeed, under mild statistical assumptions on the distribution of α_i, the sum $\sum_i \alpha_i m_i^2/r_i$ converges toward an effective average value. As the number of merged components increases, fluctuations average out and the aggregated object behaves effectively as a homogeneous configuration with a well-defined mean coefficient $\bar{\alpha}$.

As shown in Section 2.2, the contribution of individual stellar self-energies cancels exactly in the total energy balance, and does not contribute to the final expression. The resulting expression depends only on the total mass and radius of the aggregated configuration and takes the form M_n^2/R_n, up to an effective coefficient of order unity. This is precisely the functional form of the self-gravitational energy of a homogeneous solid sphere, which therefore provides a consistent effective representation of the aggregated system.

This emergence of an effective homogeneous description is a direct consequence of a law of large numbers, as microscopic structural differences are washed out at large scales.

It is important to note that the order of mergers is irrelevant, as the gravitational field is conservative. This is verified mathematically.

2.1 *Proof of permutation invariance*

Let σ be any permutation of $\{1, \ldots, n\}$. Setting:

$$M_i \equiv M_{i-1} + m_{\sigma(i)}, \qquad R_i^3 \equiv R_{i-1}^3 + r_{\sigma(i)}^3, \qquad M_0 = R_0 = 0 \tag{12}$$

we define:

$$\Delta E_i \;=\; \frac{3G}{5}\left(\frac{M_i^2}{R_i} - \frac{M_{i-1}^2}{R_{i-1}} - \alpha_{\sigma(i)} \frac{m_{\sigma(i)}^2}{r_{\sigma(i)}}\right) \tag{13}$$

The telescopic sum gives:

$$\Delta E_p = \sum_{i=1}^{n} \Delta E_i \;=\; \frac{3G}{5}\left(\frac{M_n^2}{R_n} - \sum_{i=1}^{n} \alpha_{\sigma(i)} \frac{m_{\sigma(i)}^2}{r_{\sigma(i)}}\right) \tag{14}$$

Since the sum is invariant under permutation, we obtain:

$$\sum_{i=1}^{n} \alpha_{\sigma(i)} \frac{m_{\sigma(i)}^2}{r_{\sigma(i)}} = \sum_{i=1}^{n} \alpha_i \frac{m_i^2}{r_i} \tag{15}$$

and therefore the final expression is independent of σ, which proves that $\Delta E_p = \sum_{i=1}^{n} \Delta E_i$ is invariant to the order of mergers. ■

The fact that the compact ball conserving volumes corresponds to the state of maximum total binding energy follows from the action-reaction principle and the conservation of energy. This is the most compact state that does not introduce additional repulsive forces, such as degeneracy pressure or radiation pressure, beyond those already present in the low-density state. One may think of this compact ball as a configuration in which all the stars of a galaxy are placed side by side, without introducing additional non-gravitational forces.

2.2 *Simplified calculation with identical bodies*

By assuming identical mass m, radius r, and internal structure characterized by a single coefficient α for each of the n bodies, the calculation simplifies considerably. In this case, the cumulative mass at the ith merger step is $M_i = im$, and the corresponding radius is:

$$\frac{M_i}{V_i} = \frac{m}{v} \Rightarrow R_i = \left(\frac{M_i r^3}{m}\right)^{1/3} \tag{16}$$

since M_i retains the same density as the original body of mass m.

The change in gravitational binding energy at each step is given by:

$$\Delta E_i = \frac{3G}{5}\left(\frac{M_i^2}{R_i} - \frac{M_{i-1}^2}{R_{i-1}} - \alpha\frac{m^2}{r}\right), \quad \Delta E_p = \sum_{i\leq n} \Delta E_i \tag{17}$$

Due to cancellation of intermediate terms, the telescoping sum simplifies to:

$$\Delta E_p = \frac{3G}{5}\left(\frac{M_n^2}{R_n} - \alpha n\frac{m^2}{r}\right) \tag{18}$$

Since $M_n = nm$, we find:

$$M_n^2 = n^2 m^2 \quad \text{and} \quad R_n = \left(\frac{M_n r^3}{m}\right)^{1/3} = n^{1/3} r \tag{19}$$

Substituting into the equation:

$$\Delta E_p = \frac{3G}{5}\left(\frac{n^2 m^2}{n^{1/3} r} - \alpha\frac{nm^2}{r}\right) = \frac{3G}{5}\left(n^{5/3} - \alpha n\right)\frac{m^2}{r} \tag{20}$$

It is important to note that the term proportional to αn is asymptotically subdominant compared to the leading collective contribution proportional to $n^{5/3}$. Indeed, for $n \gg 1$ and $\alpha \sim O(1)$, the ratio between the subleading and leading contributions scales as $\alpha n/n^{5/3} = \alpha n^{-2/3}$ and therefore vanishes in the large-n limit.

As a consequence, the contribution associated with the internal binding energies of the elementary bodies is negligible at leading order in the asymptotic regime. The dominant behavior is governed by the collective term M_n^2/R_n, while the detailed internal structure of the constituents contributes only through a subleading correction. This expression shows that the gravitational binding energy of the assembled system depends principally on its global mass and effective radius. Equivalently, for fixed constituent number, larger masses and smaller radii—that is, higher effective component densities—increase the collective binding energy.

The asymptotic expression obtained above corresponds to the binding energy released during the assembly of the n bodies into a single configuration. However, each individual body already possesses an intrinsic binding energy. Therefore, the total binding energy of the system must include both the interaction energy between the bodies and the intrinsic binding energy of each component. Summing over all bodies, the internal contribution is:

$$\frac{3G\,\alpha n\, m^2}{5r} \tag{21}$$

Adding this term to ΔE_p, we obtain the total binding energy:

$$E_{\text{tot}} = \Delta E_p + \frac{3G\,\alpha n\, m^2}{5r} \tag{22}$$

Substituting the expression of ΔE_p, the terms $\alpha n\, m^2/r$ and $-\alpha n\, m^2/r$ cancel exactly, yielding:

$$E_{\text{tot}} = \frac{3G}{5}\frac{M_n^2}{R_n} \tag{23}$$

The result is therefore protected in two distinct ways. First, in the assembly energy ΔE_p, the internal-structure term is already asymptotically subdominant relative to the collective contribution, since its relative weight scales as $n^{-2/3}$. Second, in the total hierarchical binding energy E_{tot}, the same internal contribution cancels exactly once the binding energies of the elementary bodies are restored.

This shows that the total binding energy of the aggregated system is identical to that of a homogeneous self-gravitating solid sphere of mass M_n and radius R_n. The contribution associated with the internal structures of the initial bodies is exactly compensated when the intrinsic binding energy of each component is included, and the final system behaves as a single continuous object whose energy depends only on its global properties. ■

2.3 *Generalization to arbitrary distributions*

The previous calculation can be generalized without assuming identical elementary bodies. Consider a system composed of n bodies with individual masses m_i, radii r_i, and internal-structure coefficients α_i. At the ith merger step, the cumulative mass and effective radius are:

$$M_i = \sum_{j=1}^{i} m_j, \qquad R_i = \left(\sum_{j=1}^{i} r_j^3\right)^{1/3} \tag{24}$$

Equivalently, the radius evolves according to:

$$R_i = \left(R_{i-1}^3 + r_i^3\right)^{1/3} \tag{25}$$

The energy released at each assembly step is then:

$$\Delta E_i = \frac{3G}{5}\left(\frac{M_i^2}{R_i} - \frac{M_{i-1}^2}{R_{i-1}} - \alpha_i \frac{m_i^2}{r_i}\right) \tag{26}$$

Summing over all merger steps again gives a telescoping series:

$$\Delta E_p = \frac{3G}{5}\left[\frac{\left(\sum_{i=1}^n m_i\right)^2}{\left(\sum_{i=1}^n r_i^3\right)^{1/3}} - \sum_{i=1}^n \alpha_i \frac{m_i^2}{r_i}\right] \tag{27}$$

Equation (27) is deterministic and does not assume any particular distribution of masses, radii, or internal structures. If the quantities (m_i, r_i, α_i) are instead regarded as random variables drawn from a probability distribution, the corresponding expectation value is:

$$\mathbb{E}[\Delta E_p] = \frac{3G}{5}\left[\mathbb{E}\left(\frac{\left(\sum_{i=1}^n m_i\right)^2}{\left(\sum_{i=1}^n r_i^3\right)^{1/3}}\right) - \mathbb{E}\left(\sum_{i=1}^n \alpha_i \frac{m_i^2}{r_i}\right)\right] \tag{28}$$

This expression is valid for any probability law for which the relevant moments exist and for which $r > 0$. In the simplest interpretation, the probability law describes a single statistically homogeneous population of components, such as a unimodal or sufficiently narrow distribution of masses, radii, and internal-structure coefficients. The distribution may then be normal, log-normal, truncated normal, empirical, or derived from a stellar mass function. No assumption of independence between m_i and r_i is required at this stage.

If the distribution is multimodal, the same formalism remains valid, but the modes should be interpreted as distinct subpopulations rather than as a single homogeneous component class. In that case, it is generally preferable to decompose the system into subpopulations with fixed asymptotic fractions and apply the same moment calculation to the corresponding mixture distribution, or equivalently to sum the contributions of each subpopulation explicitly.

If the elementary bodies are independent and identically distributed, or more generally weakly correlated with finite moments, the leading large-n behavior follows from:

$$\sum_{i=1}^n m_i \simeq n\langle m\rangle, \qquad \sum_{i=1}^n r_i^3 \simeq n\langle r^3\rangle \tag{29}$$

Therefore:

$$\mathbb{E}\left(\frac{\left(\sum_i m_i\right)^2}{\left(\sum_i r_i^3\right)^{1/3}}\right) \simeq n^{5/3}\frac{\langle m\rangle^2}{\langle r^3\rangle^{1/3}} \tag{30}$$

Similarly, the internal contribution scales as:

$$\mathbb{E}\left(\sum_{i=1}^n \alpha_i \frac{m_i^2}{r_i}\right) \simeq n\left\langle \alpha \frac{m^2}{r}\right\rangle \tag{31}$$

Thus the asymptotic expression for the expected assembly energy is:

$$\mathbb{E}[\Delta E_p] \simeq \frac{3G}{5}\left[n^{5/3}\frac{\langle m\rangle^2}{\langle r^3\rangle^{1/3}} - n\left\langle \alpha \frac{m^2}{r}\right\rangle\right] \tag{32}$$

The ratio of the internal-structure contribution to the collective contribution is therefore:

$$\frac{n\left\langle \alpha m^2/r\right\rangle}{n^{5/3}\langle m\rangle^2/\langle r^3\rangle^{1/3}} = n^{-2/3}\frac{\left\langle \alpha m^2/r\right\rangle \langle r^3\rangle^{1/3}}{\langle m\rangle^2} \tag{33}$$

For finite moments and $\alpha \sim O(1)$, this ratio vanishes as $n^{-2/3}$. Hence, the suppression of the internal-structure term is not a consequence of the simplifying assumption of identical bodies. It persists for arbitrary component distributions satisfying the stated moment conditions.

Finally, if the internal binding energies of the initial components are added back to the assembly energy, Eq. (27) gives the exact cancellation:

$$E_{\rm tot} = \Delta E_p + \frac{3G}{5}\sum_{i=1}^n \alpha_i \frac{m_i^2}{r_i} = \frac{3G}{5}\frac{\left(\sum_{i=1}^n m_i\right)^2}{\left(\sum_{i=1}^n r_i^3\right)^{1/3}} \tag{34}$$

Thus the same double protection remains in the general case. The internal contribution is both asymptotically subdominant in the assembly energy and exactly compensated in the final total binding energy. Consequently, the leading gravitational energy of the aggregated system is controlled by the global mass and effective radius, not by the microscopic details of the initial constituents. ■

2.4 *Hierarchical calculation of binding energy*

We have established in Sections 2.2 and 2.3 that the leading binding energy of an aggregated system is governed by its total mass and effective radius. This result can now be applied to stellar populations grouped into classes within a galaxy.

For each stellar class i, let M_i, V_i, and R_i denote respectively the total mass, total effective volume, and

effective radius of the class. The effective radius is obtained from the total volume of the stellar components in that class. If v_{ik} denotes the volume of the kth star in class i, then:

$$V_i = \sum_{k=1}^{N_i} v_{ik} \simeq N_i \langle v \rangle_i, \qquad R_i = \left(\frac{3V_i}{4\pi} \right)^{1/3} \tag{35}$$

Equivalently, if one introduces an effective density ρ_i for the class, it should be understood as a derived quantity:

$$\rho_i = \frac{M_i}{V_i} \simeq \frac{\langle m \rangle_i}{\langle v \rangle_i}, \qquad R_i = \left(\frac{3M_i}{4\pi\rho_i} \right)^{1/3} \tag{36}$$

The previous equation (34) gives the internal binding energy of each stellar class. The total class-level contribution is then obtained by summing over all classes:

$$E_{\rm sum} = \frac{3G}{5} \sum_{i=1}^{n} \frac{M_i^2}{R_i} \tag{37}$$

and applying Equation (14) exactly as in Section 2.2, with:

$$M = \sum_{i=1}^{n} M_i \qquad \text{and} \qquad R = \left(\sum_{i=1}^{n} R_i^3 \right)^{1/3}$$

so that R is the radius of the aggregated solid sphere obtained by volume conservation, gives:

$$\Delta E_p = \sum_{i=1}^{n} \Delta E_i \;=\; \frac{3G}{5} \left(\frac{M^2}{R} - \sum_{i=1}^{n} \alpha_i \frac{M_i^2}{R_i} \right) \tag{38}$$

This would lead to identifying the total energy with the single term $(3G/5)\, M^2/R$. However, empirically, one finds:

$$\frac{3G}{5} \frac{M^2}{R} < \frac{3G}{5} \sum_{i=1}^{n} \frac{M_i^2}{R_i} \tag{39}$$

which is experimentally verified using SPARC galaxies, with discrepancies spanning approximately 1% to 10%.

Thus, if $(3G/5) \sum_{i=1}^{n} M_i^2/R_i$ correctly represents the energy emitted as radiation during inelastic collisions, that is, during the fusion of all stars of identical density and mass within each class, then the energy emitted by the fusion of the remaining aggregated solid spheres should be larger, not smaller.

Accordingly, the complete form of the estimator should instead be:

$$E_{\rm tot} = \frac{3G}{5} \sum_{i=1}^{n} \frac{M_i^2}{R_i} + \Delta E_p \tag{40}$$

with $\Delta E_p > 0$.

2.5 *Correct Newtonian derivation*

The previous difficulty comes from an incorrect construction of the second aggregation step. In the first step, stars of similar intrinsic density are merged into homogeneous class-level compact spheres. In the second step, these compact spheres were then treated as if they could be merged again in the same way to obtain the total released energy. However, in both cases the Newtonian expression gives an energy difference between two states. It gives the energy of the compact final state minus the energy already contained in the smaller compact initial states.

The class-level spheres obtained from Equation (36) are therefore not quantities that must be subtracted away from the final result. They are part of the final hierarchical configuration. The real final state is a global compact sphere made by aggregating homogeneous class-level compact spheres. Its total binding energy is therefore the sum of the binding energies of these smaller compact spheres, given by Equation (37), plus the aggregation energy of these compact spheres inside the global object.

In principle, this second contribution could be calculated by summing the $(n^2 - n)/2$ gravitational relations between the class-level compact spheres. A simpler Newtonian approximation is obtained by considering that many compact spheres are distributed without a preferred ordering, so that one can pass to the continuum limit. In this limit, the aggregation energy has the same functional form as the binding energy of a homogeneous compact sphere with total mass M and volume-conserving radius R.

The final Newtonian hierarchical binding energy is therefore:

$$E_p = \frac{3G}{5} \left[\sum_{i=1}^{n} \frac{M_i^2}{R_i} + \frac{M^2}{R} \right] \tag{41}$$

Strictly speaking, each Newtonian aggregation step contains a subtraction term of the form $\sum_i m_i^2/r_i$ for the stars. As shown in Section 2.2, this term is both asymptotically negligible and exactly cancelled when the intrinsic stellar binding energies are included in the total energy budget. It therefore does not appear as an additional contribution in Equation (41).

The first term is the binding energy already stored in the homogeneous class-level compact spheres. The second term is the additional aggregation energy of these compact spheres into the global compact configuration. Thus, the two-term structure follows from a correct Newtonian accounting of the final hierarchical state.

At first sight, the global aggregation term used in the empirical evaluation below may appear to be a

crude approximation, since the numerical implementation represents the stellar population with only eleven classes. However, this term is not controlled by the number of stellar classes used in the parametrization. It represents the continuum-limit aggregation energy of the compact class-level subsystems, and the calculation may therefore be understood as the limit in which the number of such subsystems becomes large.

It is worth noting that the Newtonian hierarchical form derived in Equation (41) is the same two-term expression introduced in Poupart (2026).

We now use this result as a consistency test of the proposed energy form. If the Newtonian hierarchical construction captures the correct structure of the binding energy, then allowing the two contributions to vary independently should not lead to an arbitrary parameter dependence. Instead, the empirical exploration should reveal whether the data favor the relative weights predicted by the model, or whether deviations from these weights indicate that the formulation is incomplete. We therefore consider the generalized estimator:

$$E_p = \frac{3G}{5}\left[\alpha \sum_{i=1}^{n} \frac{M_i^2}{R_i} + \beta \frac{M^2}{R}\right] \tag{42}$$

and study experimentally how variations in the parameters α and β affect the agreement with observational data.

2.6 *Recursive interpretation of the hierarchical energy*

The Newtonian derivation above shows that the two-term estimator is not obtained by erasing the intermediate levels of the construction. The class-level compact spheres already contain binding energy, and the global term represents the additional aggregation energy of these compact subsystems into the final volume-conserving configuration.

This gives a direct recursive interpretation of the energy. Let S denote a system decomposed into subsystems S_i. If the subsystems have already been formed, their binding energies are part of the energy content of the final hierarchical state. They must therefore enter the next level of the construction with unit weight. The only new contribution at this level is the aggregation energy of the subsystems into the larger compact configuration. The recursive energy can therefore be written as :

$$F(S) = \sum_i F(S_i) + \beta B(S)$$

where

$$B(S) = \frac{3G}{5}\frac{M^2}{R}$$

The coefficient of the first term is fixed by the recursive construction itself. Changing it would mean that the binding energies already stored in the subsystems are either partially erased or artificially amplified when the next aggregation level is formed. No such operation occurs in the Newtonian construction. For this reason, the natural recursive value of the class-level coefficient is $\alpha = 1$.

For stellar population classes, each subsystem S_i has mass M_i, effective radius R_i, and class-level binding-energy contribution:

$$F(S_i) \simeq \frac{3G}{5}\frac{M_i^2}{R_i}$$

Substituting these class-level contributions into the recursive expression gives:

$$F(S) = \frac{3G}{5}\left[\sum_{i=1}^{n} \frac{M_i^2}{R_i} + \beta \frac{M^2}{R}\right]$$

Thus, the recursive interpretation selects $\alpha = 1$ as the value required when class-level compact spheres are treated as real subsystems whose binding energies are retained in the final hierarchical state.

In this interpretation, the term proportional to α is not a residual contribution from individual stellar self-energies. These individual terms are negligible at large N, scaling as $N^{-2/3}$ relative to the collective class energy. Rather, the term:

$$\sum_{i=1}^{n} \frac{M_i^2}{R_i}$$

represents the binding energy of the stellar population classes themselves as physically distinct hierarchical subsystems. The parameter α therefore measures whether these class-level contributions are retained in the total effective energy. The recursive construction retains them with unit weight, giving the natural value $\alpha = 1$.

2.7 *Relativistic consistency bound*

The preceding Newtonian derivation defines the energy of compact reference configurations. This construction is valid as long as the equivalent compact sphere can be interpreted as a physically meaningful material configuration. When the compactness becomes too large, however, the equivalent radius approaches the Schwarzschild radius and the Newtonian compact-sphere estimate can no longer be interpreted literally.

For a self-gravitating solid sphere, the Newtonian binding-energy scale is:

$$B_E = \frac{3G}{5}\frac{M^2}{R} \tag{43}$$

which corresponds to an effective mass contribution:

$$M_{B_E} = \frac{B_E}{c^2} = \frac{3G}{5}\frac{M^2}{c^2 R} \tag{44}$$

The ratio between this contribution and the total mass is therefore:

$$\frac{M_{B_E}}{M} = \frac{3G}{5}\frac{M}{c^2 R} \tag{45}$$

This ratio measures the relative importance of gravitational self-energy in the total energy budget. When it becomes non-negligible, the assumptions of the weak-field approximation break down, as gravitational energy itself contributes to the source of the field.

Rewriting this condition in terms of the Schwarzschild radius $R_S = 2GM/c^2$, one finds that:

$$\frac{M_{B_E}}{M} = \frac{3}{10}\frac{R_S}{R} \tag{46}$$

so that the breakdown of the weak-field approximation occurs for $R \lesssim R_S$. In particular, when $M_{B_E}/M \gtrsim 3/10$, the system enters a relativistic regime where this approximation is no longer valid.

A more restrictive constraint can be obtained by combining this expression with the Buchdahl bound, which imposes $R > 9GM/(4c^2) = 9R_S/8$ under the usual assumptions of a static, spherically symmetric, isotropic fluid configuration. Substituting this lower limit into (46):

$$\frac{M_{B_E}}{M} = \frac{3}{10}\frac{R_S}{R} < \frac{3}{10}\frac{8}{9} = \frac{4}{15} \tag{47}$$

This shows that the Newtonian estimate cannot be extrapolated arbitrarily, and that the transition to a fully relativistic description necessarily occurs before the gravitational self-energy becomes comparable to the total mass. The Buchdahl bound therefore marks the limit beyond which the weak-field approximation breaks down and a general relativistic treatment is required.

2.8 *Recursive absorption and the black-hole limit*

The relativistic consistency bound defines the domain in which the compact reference configuration can be interpreted as a material state, namely $R > R_s$. However, it does not by itself determine whether the same energy-accounting function can remain valid when the system is considered as being absorbed sequentially by a black hole. The relevant point is therefore not to assign internal structure to a black hole, but to determine whether the functional form obtained in the Newtonian regime remains stable under successive absorption events.

In the Newtonian regime, as long as the equivalent compact radius satisfies $R > R_s$, the hierarchical construction gives a well-defined absorbed-energy function. This applies in particular to the absorption of external bodies by an already formed black hole, provided the calculation is performed outside the horizon.

If this function correctly describes one absorption step, it should not cease to apply at the next step merely because the black hole has absorbed one additional component. After each absorption event, the final object is again a black hole characterized only by its global parameters. By the no-hair property, the detailed composition and assembly history are no longer observable degrees of freedom. Therefore, any modification of the absorption law would have to arise from a new global physical criterion, not from the disappearance of internal substructure.

This is precisely what the recursive form expresses. Let B_k denote the global compact contribution after k absorbed subsystems:

$$B_k = \frac{3G}{5}\frac{M_k^2}{R_k}$$

and let F_k denote the total effective energy after these k subsystems have been included. If the recursive form holds at step k:

$$F_k = \sum_{i=1}^{k} F_i + \beta B_k$$

then adding one additional subsystem gives:

$$F_{k+1} = F_k + F_{k+1}^{\text{class}} + \beta\,(B_{k+1} - B_k)$$

Substituting the expression for F_k gives:

$$F_{k+1} = \sum_{i=1}^{k} F_i + \beta B_k + F_{k+1}^{\text{class}} + \beta\,(B_{k+1} - B_k)$$

and therefore:

$$F_{k+1} = \sum_{i=1}^{k+1} F_i + \beta B_{k+1}$$

The recursive form is therefore stable under sequential absorption. ■

The no-hair property supports this interpretation. The class-level terms do not represent persistent observable structures inside the final black hole. They represent energy contributions carried by the absorbed

subsystems before they are incorporated into the global mass–energy budget. Once absorption has occurred, these contributions are no longer distinguishable as separate components, but the total energy balance still contains them.

This shows that the recursive form is formally stable under sequential absorption and therefore provides a natural continuation of the Newtonian energy-accounting function toward a relativistic absorption limit. The black-hole case is used here only as a limiting test, since the final object need not retain the absorbed stellar classes as separate structures, while the total absorbed energy may still follow the same hierarchical functional form. In this sense, the recursive construction provides a coherent way to understand why a non-zero class-level contribution can remain compatible with a general-relativistic mass–energy balance, and why the natural recursive value is $\alpha = 1$.

2.9 *Homogeneous aggregation and the virial factor*

This provides a natural interpretation of why the two terms in the estimator need not carry the same coefficient. The first term is obtained by aggregating objects that belong to the same stellar class and therefore share the same intrinsic density. Under volume conservation, this operation produces an equivalent compact sphere of the same density, with:

$$R_i^3 = \sum_j r_{ij}^3, \qquad M_i = \sum_j m_{ij}$$

In this case, the class-level contribution is naturally described by the full compact-sphere binding term:

$$B_i = \frac{3G}{5}\frac{M_i^2}{R_i}$$

This supports the recursive value $\alpha = 1$, since the first term represents the binding energy of homogeneous class-level subsystems.

The global term has a different status. It combines stellar classes with very different intrinsic densities into a single effective radius defined by:

$$R^3 = \sum_i R_i^3$$

The distinction between the two coefficients therefore reflects the difference between homogeneous aggregation within stellar classes and heterogeneous aggregation between classes.

This object should not be interpreted as a truly homogeneous solid sphere of fixed density. It is instead closer to an effective gravitational aggregate of heterogeneous subsystems. For such a self-gravitating aggregate, the relevant bound energy need not be the full magnitude of the Newtonian potential term. If the global configuration is interpreted as virialized, with $U = -B$ and $2K + U = 0$, then the total mechanical binding energy is:

$$|E| = \frac{B}{2}, \qquad B = \frac{3G}{5}\frac{M^2}{R}$$

This provides a natural physical motivation for $\beta \simeq 1/2$.

Thus, the distinction between the two coefficients is not arbitrary. The coefficient α applies to homogeneous compact class-level contributions, for which the full binding term is retained, while β applies to the global heterogeneous aggregation, where a virial factor can reduce the effective contribution by one half. This gives a coherent interpretation of the empirically favored form with $\alpha \simeq 1$ and $\beta \simeq 1/2$.

3. Comparison of binding energy estimators

We now compare a family of gravitational binding-energy estimators by testing their ability to reproduce both the effective dark mass inferred from galactic dynamics and the photometric ordering of galaxies. The comparison follows the reconstruction strategy introduced in Poupart (2026), in which stellar populations are reconstructed from dynamical constraints alone, and the resulting predicted colors are compared a posteriori with observations.

We consider a two-parameter family of estimators of the form:

$$E_p(\alpha,\beta) = \frac{3G}{5}\left[\alpha \sum_{i=1}^{n} \frac{M_i^2}{R_i} + \beta\frac{M^2}{R}\right] \tag{48}$$

where the first term represents the additive contribution of the different stellar population classes, while the second term represents the global compact configuration obtained after volume-conserving aggregation. The parameters α and β therefore control the relative weights assigned to the class-level binding-energy contribution and the global binding-energy contribution. For each stellar class i, the effective radius is defined by its total mass M_i and intrinsic density ρ_i:

$$R_i = \left(\frac{3M_i}{4\pi\rho_i}\right)^{1/3} \tag{49}$$

while the global radius is obtained from volume conservation:

$$R^3 = \sum_{i=1}^{n} R_i^3 \tag{50}$$

The predicted effective dark mass is then defined through mass–energy equivalence:

$$M_{\rm dark}^{\rm pred} = \frac{E_p(\alpha,\beta)}{c^2} \tag{51}$$

The reconstruction is performed using the SPARC database Lelli *et al.* (2016). For each galaxy, the only dynamical inputs are the baryonic mass $M_{\rm bar}$ and the effective dark mass $M_{\rm dark}$ inferred from the rotation curve. No photometric information is used during the reconstruction.

The reconstruction algorithm and its statistical validation are described in detail in the companion paper (Poupart, 2026). This includes the stellar population basis, initial fractions and dispersions, stopping criteria, no-search baselines, random-initialization tests, search-strategy comparisons, gas-clumping tests, and radial robustness checks. Here, the same framework is used as a fixed diagnostic tool to compare the family of binding-energy estimators parameterized by (α,β).

The stellar population basis consists of compact remnants and main-sequence stellar classes:

BH, NS, WD, RG, M, K, G, F, A, B, O.

Each component is assigned an initial mass fraction $\phi_i^{(0)}$ and an allowed dispersion σ_i. The fractions are normalized so that:

$$\sum_{i=1}^{n} \phi_i = 1 \tag{52}$$

During the reconstruction, each fraction is constrained to remain within:

$$\max\!\left(0,\ \phi_i^{(0)} - k\sigma_i\right) \le \phi_i \le \min\!\left(1,\ \phi_i^{(0)} + k\sigma_i\right) \tag{53}$$

with $k = 3$.

For each pair (α,β), the stellar fractions are optimized using a greedy reconstruction algorithm. At each iteration, candidate moves are generated by perturbing one fraction at a time:

$$\phi_i \to \phi_i + \delta_i, \qquad \delta_i \in \{-\lambda\sigma_i,\ +\lambda\sigma_i\} \tag{54}$$

followed by renormalization of the full fraction vector. Candidate moves that violate the admissible bounds are rejected.

Each admissible move is evaluated by the relative error:

$$\mathcal{E}(\boldsymbol{\phi}) = \frac{\left|M_{\rm dark}^{\rm pred}(\boldsymbol{\phi}) - M_{\rm dark}\right|}{M_{\rm dark}} \tag{55}$$

The selected move is the one that minimizes the dynamical error among all admissible candidates. If no improving move is found, the step size λ is reduced, and the search continues until the minimum exploration scale is reached.

A gas clumping parameter κ can also be introduced as an additional degree of freedom. In that case, the effective baryonic mass entering the binding-energy estimator is written:

$$M_{\rm eff} = M_{\rm bar}(1-\kappa) \tag{56}$$

with $\kappa \in [0,1]$. When no further improvement can be obtained by changing the stellar fractions, the algorithm scans κ and retains the value that minimizes the dynamical error.

Once the stellar population has been reconstructed, its integrated photometric properties are computed using standard stellar population synthesis prescriptions. The predicted colors are then compared with GALEX Martin *et al.* (2005) and SDSS York *et al.* (2000) observations for the color indices FUV–NUV, NUV–r, $g-r$, and $r-z$.

The photometric agreement is quantified using Pearson and Spearman correlations between predicted and observed colors. Pearson coefficients measure linear agreement, while Spearman coefficients measure monotonic ordering. The dynamical agreement is quantified directly from the relative error between the predicted and observed effective dark masses.

The grid exploration over (α,β) therefore evaluates two independent properties of each estimator: its ability to reproduce the effective dark mass inferred from rotation curves, and its ability to recover the observed photometric ordering of galaxies without using photometric information during the reconstruction. This provides a direct test of whether a given binding-energy estimator carries physically relevant information about both the dynamical mass budget and the underlying stellar population structure.

3.1 *Photometric score exploration*

The photometric score studied here is defined as the product of the signed sums of the Pearson and Spearman significances over all colors (FUV-NUV, NUV-r, g-r, r-z). The sums are constructed using the sign of the correlation, yielding sum_P for Pearson and sum_S for Spearman. The final score is defined as:

$$\mathrm{score} = \max(\mathrm{sum}_P, 0) \cdot \max(\mathrm{sum}_S, 0) \tag{57}$$

This construction neutralizes positive significances when they are compensated by negative correlations. Any negative score is set to zero.

The score is evaluated as a single global quantity for each point of the (α,β) grid, combining the correlation information obtained from all available photometric colors. Depending on the color index, the number of galaxies entering the correlations ranges from approximately $N \simeq 120$ to $N \simeq 140$, as determined by the overlap between GALEX and SDSS datasets.

For visualization purposes, the scores displayed in the grid maps are normalized to the interval $[0, 1]$, with 1 corresponding to the best coarse-grid raw score, 878 at $(\alpha,\beta) = (1, 3)$. Unless explicitly stated otherwise, all numerical scores reported below are raw scores.

The resulting exploration of the (α,β) parameter space with $\Delta = 0.1$ is shown in Figures 1-4. The Figure 1 shows the normalized score over the parameter space. The Figure 2 displays the local average contrast, enhancing variations between neighboring cells. The Figure 3 highlights the five maximum scores for each α in light gray and the five maximum scores for each β in dark gray, with overlaps shown in black. The Figure 4 represents a direction field indicating the orientation of local increase in the score.

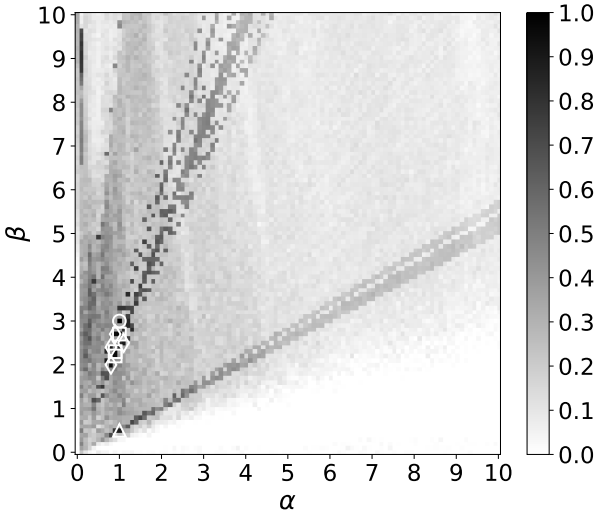

Figure 1. Original normalized grid showing the photometric score values across the (α,β) parameter space.

A prominent feature of these maps is the presence of two well-defined linear structures. The first passes through $(1, 5/2)$ with an approximate slope of $5/2$, while the second passes through $(1, 1/2)$ with an approximate slope of $1/2$. The nine highest-scoring solutions (white symbols) lie along these two lines, a property that remains valid when extending the analysis to the top one hundred configurations, with the additional appearance of solutions along a more diffuse structure in the upper-right region with a slope of approximately 10. The highest-scoring configuration is

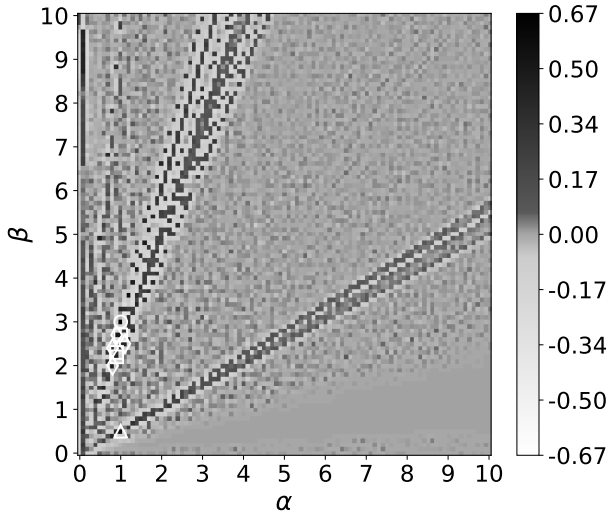

Figure 2. Local photometric score difference map relative to neighboring cells.

located at $(1, 3)$, with most other top-ranked solutions clustered around $\beta = 2.5$, except for the ninth-best solution, which lies at $(1, 1/2)$. It is clear that the highest-scoring solutions are therefore grouped at the intersection of these lines and the line $\alpha = 1$.

Not only do the highest-scoring solutions cluster along these lines, but they also follow a clear gradient on alpha. The fifty maximum scores are found at $\alpha \leq 2$, the two hundred and fifty maximum scores at $\alpha \leq 3$, and the five hundred maximum scores at $\alpha \leq 4$.

These same linear structures also contain some of the worst-performing configurations, indicating that they do not correspond to regions of uniformly high score, but rather organize the full range of solutions across the parameter space.

At first sight, these structures could be interpreted as iso-energy lines. However, this interpretation is incorrect. For a function of the form $f(\alpha,\beta) = \alpha A + \beta B$, there exists only a single family of linear level sets. Moreover, the observed structures do not share the same thickness or distribution of high-scoring configurations, which further excludes a simple iso-energy interpretation.

These lines therefore reflect the structure of the photometric reconstruction quality produced by the algorithm as a function of (α,β); they are not properties of the estimator itself.

3.2 *Dynamical score exploration*

The dynamical score studied here is defined from the relative error between the predicted and observed dynamical quantities. For each galaxy, a relative error ϵ is

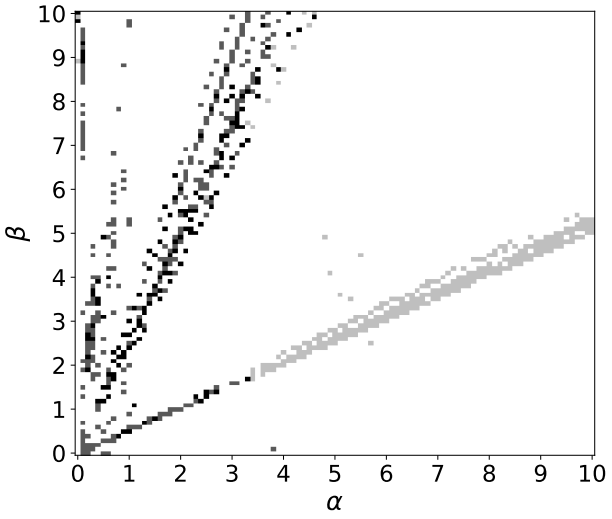

Figure 3. Regions selected among the top 5 photometric score values per α (light gray) and per β (dark gray), with overlap shown in black.

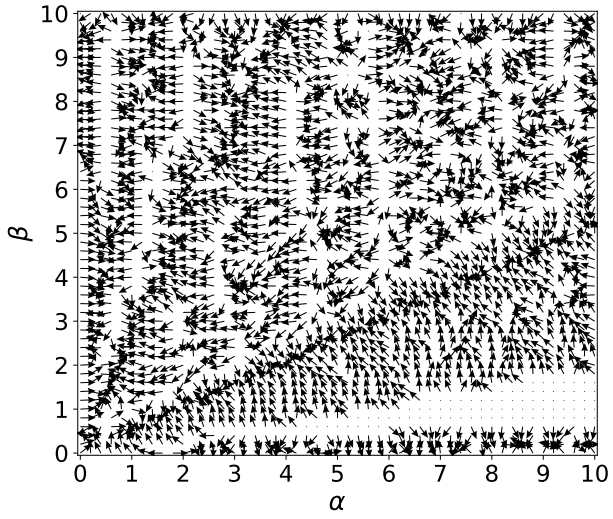

Figure 4. Ascent direction field indicating the local trend toward higher photometric score values in parameter space.

computed, and a global error is obtained by averaging over the full sample of $N = 174$ galaxies.

This global error is then normalized over the (α, β) grid, yielding a dimensionless quantity $\epsilon_{\rm norm} \in [0, 1]$. The score is defined as its complement, score $= 1 - \epsilon_{\rm norm}$, so that higher values correspond to better agreement with the observed dynamics.

The score is therefore evaluated as a single global quantity for each point of the (α, β) grid with $\Delta = 0.1$. Figures 5–8 are the same as those presented in the previous sections 3.1.

Figure 7 shows that the selection map of the five highest-scoring solutions per α and per β reveals a structure that is markedly different from the photometric case. The best-performing models tend to favor configurations dominated by a single term, either the α or the β contribution, rather than a balanced combination of both. When both terms are retained, the only noticeable overlap region is confined to the lower-right corner of the parameter space, near $(0, 0)$.

However, in the local-contrast map shown in Figure 6, the same linear structures observed in the photometric maps reappear in the dynamical case. This indicates that, although the global behavior is largely governed by either α or β, these lines still organize the variations in reconstruction quality across the parameter space. As in the photometric case, they contain both high- and low-quality solutions, demonstrating that they do not correspond to uniformly optimal regions but rather to underlying structural features of the solution space. It is also worth noting that these two lines are part of a broader family of rays emanating from the origin.

Furthermore, the nine highest-scoring solutions, shown as white symbols in Figure 5 and as black symbols in Figure 6, are also located approximately along these lines, but appear compressed along the vertical direction and slightly offset downward. This reflects the dominance of the α gradient, which partially masks the signal associated with these structures. Nevertheless, this signal remains more pronounced than the variations induced by the β gradient (see Figure 8).

3.3 *Statistical significance and population grouping*

The statistical differences between the photometry generated by the best parameter points, such as $(\alpha, \beta) = (1, \frac{1}{2})$ and $(\alpha, \beta) = (1, 3)$, rarely exceed $|\Delta_\sigma| > 1$ and never reach $|\Delta_\sigma| > 2$. This is expected when two rankings are practically indistinguishable from random fluctuations. Consequently, Pearson and Spearman correlation coefficients alone do not allow one to decide which of these parameter points is genuinely superior.

It is nevertheless possible to compare the stellar populations inferred with $(\alpha, \beta) = (1, \frac{1}{2})$ to those inferred with $(\alpha, \beta) = (1, 3)$ by using the available GALEX and SDSS photometry. For each galaxy, a local score function is computed between the predicted and observed bands, allowing one to define an "optimal" value of β as the one producing the best local score.

This local selection reveals a structure that is almost invisible in the global correlation coefficients. In the subset of galaxies with sufficient photometric coverage, the sample separates into two empirical groups.

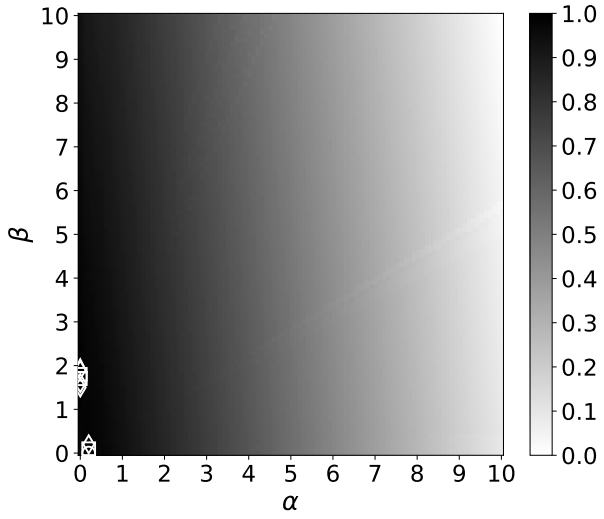

Figure 5. Original normalized grid showing the dynamical score values across the (α, β) parameter space.

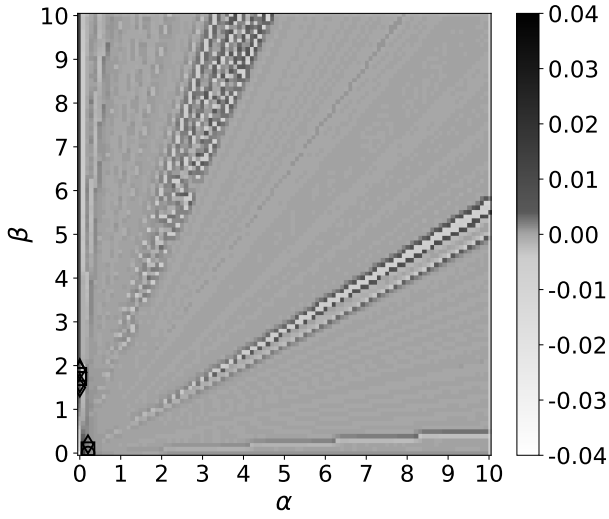

Figure 6. Local dynamical score difference map relative to neighboring cells.

A total of 40 galaxies prefer $\beta = \frac{1}{2}$, while 101 galaxies prefer $\beta = 3$. This separation is not randomly distributed among morphological types. Early and intermediate spiral galaxies, from S0 to Sc, almost always select the high-β branch, with only 2 galaxies out of 51 in this range preferring $\beta = \frac{1}{2}$. In contrast, late-type and dwarf systems, from Scd to BCD, contain 38 of the 40 galaxies associated with $\beta = \frac{1}{2}$. In this latter group, the fraction of galaxies preferring $\beta = \frac{1}{2}$ reaches approximately 42%, whereas it is only about 4% among earlier and more regular morphologies.

This morphological correlation indicates that the small differences between the two photometric solutions are not purely random. The local preference for $\beta = 3$ is mainly associated with more structured spiral galaxies, where the baryonic distribution is more concentrated and where the stellar and gaseous components may play more differentiated roles. The local preference for $\beta = \frac{1}{2}$ appears preferentially in late-type, irregular, or compact systems, which are often more gas dominated and less morphologically organized.

The first remarkable observation is that none of the 40 galaxies with $\beta = \frac{1}{2}$ requires gas clumping, whereas 53 of the 101 galaxies with $\beta = 3$ do. Applying an exact test of independence to these two groups gives a significance of approximately 6.4σ.

This correlation is not a trivial consequence of the fitting procedure. In the present model, gas clumping is introduced when the energy function $E(M_{\rm bar})$ generates too much effective dark mass. The clumped fraction of the gas is then removed from the effective baryonic contribution in order to reduce the generated mass. However, for the same baryonic mass, $\beta = 3$ generates more effective dark mass than $\beta = \frac{1}{2}$. One would therefore naively expect galaxies requiring gas clumping to avoid the larger value of β, not to prefer it. The observed association between gas clumping and $\beta = 3$ is therefore directionally counter-intuitive, making the correlation more significant rather than less significant. It indicates that the local preference between $\beta = \frac{1}{2}$ and $\beta = 3$ is linked to the structure of the baryonic distribution, even though this does not by itself justify two different energy functions.

The second remarkable observation is that using the locally optimal value of β, either $\frac{1}{2}$ or 3, for each individual galaxy does not improve the global Pearson or Spearman correlation coefficients over the full sample. This may seem paradoxical, but it follows naturally from the difference between local and global optimization. The optimal β is selected galaxy by galaxy from a local photometric score, whereas Pearson and Spearman measure global properties of the complete population. Pearson is mainly sensitive to the global linear relation between two distributions, while Spearman is sensitive to the relative rank ordering of all galaxies. Neither quantity is guaranteed to improve when independent local choices are made.

In particular, an improvement in the photometric score of a single galaxy may be too small to change its position in the global ordering. It may also modify the local residuals without improving the rank structure of the full sample. When two solutions are already nearly degenerate, the residual differences between $\beta = \frac{1}{2}$ and $\beta = 3$ can behave like classification noise from the point of view of a global ranking statistic. They may identify the better solution for an individual galaxy while failing

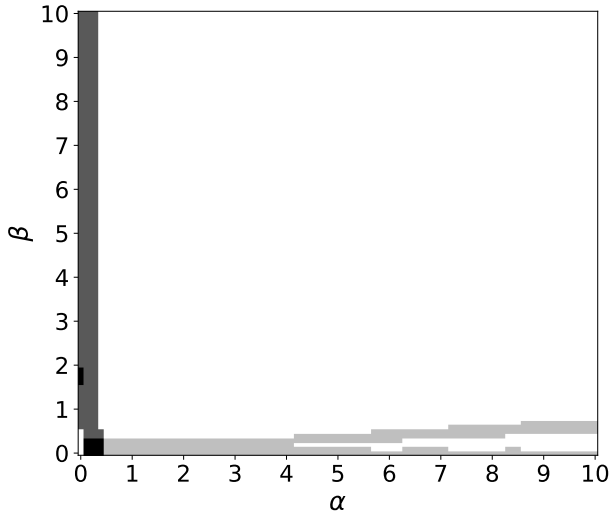

Figure 7. Regions selected among the top 5 dynamical score values per α (light gray) and per β (dark gray), with overlap shown in black.

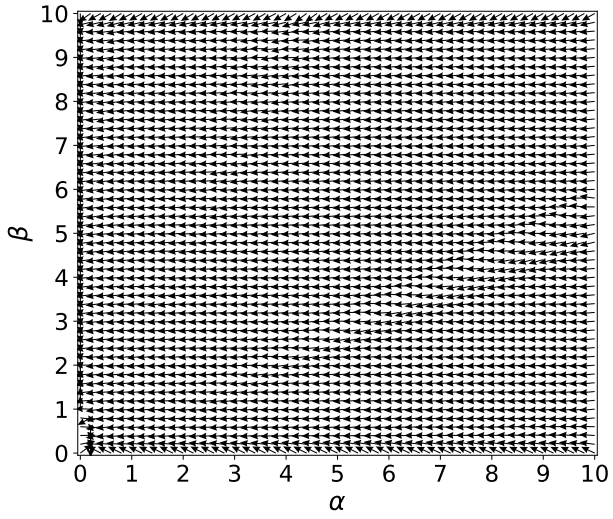

Figure 8. Ascent direction field indicating the local trend toward higher values in parameter space.

to produce a coherent monotonic transformation of the entire population. This limitation is especially important for Spearman's coefficient, since it depends on the relative ordering of all galaxies rather than on the absolute quality of each individual fit. An algorithm that only has access to the current galaxy cannot, in general, be expected to maximize a global rank-based criterion.

The conclusion is therefore deliberately conservative. The statistical differences between the two values of β are insignificant at the level of individual photometric ranking. These small differences nevertheless correlate clearly with morphology and gas clumping. However, they do not justify the introduction of two distinct energetic regimes or two different energy functions, since this usage does not improve the global Pearson or Spearman correlations. Consequently, the hypothesis that a single real energy function, and therefore a single value of β, applies to all galaxies remains fully justified, although not confirmed by the present analysis.

3.4 *Synthesis*

The existence of similar structural patterns in both the dynamical and photometric maps points to an underlying organizing property of the reconstruction. In both cases, the common object is the reconstructed stellar population, but the two evaluated quantities are mathematically very different.

For the dynamical score, the stellar population enters through the gravitational binding-energy estimator, which maps the mass fractions and intrinsic densities of the stellar classes to an effective dark mass, compared to the value inferred from SPARC rotation curves. For the photometric score, the same reconstructed population enters through its predicted colors, obtained from the luminosity contribution of the different stellar components and compared to observed GALEX and SDSS colors.

There is no a priori reason why these two mappings should produce the same structures in the (α,β) parameter space. One mapping depends on gravitational energy and density-dependent mass terms, while the other depends on stellar luminosities and colors. The fact that both reveal similar linear structures therefore cannot be interpreted as a trivial consequence of the parametrization alone.

The most natural interpretation is that these structures reflect an underlying physical organization of the stellar population mixtures themselves. In other words, the same regions and directions in the (α,β) space correspond to population configurations that are simultaneously meaningful for the dynamical reconstruction and for the photometric prediction.

This does not imply that the structures are uniformly optimal. On the contrary, they contain both good and poor solutions. The same behavior is observed in both the photometric and dynamical analyses. Even when these structures are partially masked by dominant gradients in the dynamical maps, the highest-scoring solutions systematically appear near the extremities of the corresponding lines.

These structures should therefore be understood as organizing features of the solution space, along which the reconstruction explores a continuum of stellar pop-

ulation configurations, spanning from poor to optimal agreement. The same structures are recovered in both photometric and dynamical analyses, even though the two diagnostics depend on distinct mappings of the reconstructed stellar populations. This consistency indicates that the result is not a trivial numerical artifact, but reflects underlying constraints imposed by the stellar population distributions, which are captured in both observables. In other words, these structures reflect the underlying physical reality of both good and poor stellar population reconstructions.

4. Candidate forms of the estimator

We now identify candidate values for the parameters (α, β) based on the previous analysis.

A first guiding principle is that the binding-energy formulation should ultimately admit a rigorous analytical derivation, for instance within a relativistic framework. If such a derivation exists, it is natural to expect that the coefficients α and β would take simple fractional values, rather than arbitrary real numbers.

From the empirical exploration, the highest-scoring photometric solution is found at $(1, 3)$, and belongs to a cluster of the eight highest-scoring configurations centered around $(1, \frac{5}{2})$.

However, another distinct branch is revealed by the ninth-best solution, located at $(1, \frac{1}{2})$. Interestingly, this second branch is favored by the dynamical analysis, where the highest-scoring solutions is obtained at low α and low β.

A detailed exploration of the parameter space at a resolution of $\Delta = 10^{-3}$ was not computationally feasible with the resources available. Instead, a refined exploration was performed over the restricted region $\alpha \in [0, 3]$ and $\beta \in [0, 6]$, which contains the main high-quality structures identified in Figure 1.

This refined region was divided into 325 subgrids. Each subgrid contained 25×25 sampled points, corresponding to a local resolution of $\Delta = 10^{-2}$. The refined exploration therefore included a total of $325 \times 25 \times 25 = 203\,125$ sampled points.

The best raw score found in the refined-grid exploration is 988 at $(0.87, 2.02)$. Restricting the refined-grid exploration to solutions with a raw score above 850, only 407 points satisfy this criterion, corresponding to approximately 0.2% of the sampled configurations. These points are further localized within 23 subgrids out of 325, i.e. approximately 7.1% of the explored regions.

Focusing on the two subgrids containing the highest-scoring solutions, with raw scores of 988 and 984 respectively, the distribution of normalized scores within these regions exhibits mean and standard deviation of 55% ± 24% and 57% ± 24%. The average raw score of a randomly selected point within these subgrids exceeds 540, which is substantially higher than the score of 367 obtained for $(\alpha, \beta) = (1, 1)$ in our previous study Poupart (2026).

However, this richness also complicates the identification of parameter values that could correspond to a simple analytical form. Numerous linear substructures appear within these regions, forming band-like patterns in which the ordering of the scores does not follow any clear trend. Within these bands, the distribution of values appears irregular, with no simple fractional values emerging, nor any clustering around a specific preferred value.

Caution is required when interpreting such refinements. The model relies on a discretized description of stellar populations using eleven classes, each characterized by a representative density specified with only two significant digits. This limited precision inherently constrains the meaningful accuracy of the parameters (α, β), and prevents over-interpreting small deviations from simple fractional values.

Taken together, the exact parameter values $(1, 3)$ and $(1, \frac{1}{2})$, with raw scores of 878 and 779 respectively, remain natural candidates, since they are also present in the refined exploration and are surrounded by high-scoring nearby configurations. The highest-scoring solutions in the respective refined subgrids containing these two values are found at $(0.99, 0.51)$ with a raw score of 866, and at $(1, 3.02)$ with a raw score of 927, respectively.

Among these, the point $(1, \frac{1}{2})$ is of particular interest. Although the best refined point in the local neighborhood of $(1, \frac{1}{2})$ reaches a raw score of 866, ranking only fifth among the 23 selected high-score subgrids, the exact fractional point $(1, \frac{1}{2})$ satisfies several independent criteria:

(A) The point $(1, \frac{1}{2})$ lies within one of the two main linear structures identified in the coarse-resolution maps. It is also unique among the 25 highest-scoring points, being the only one located on this structure, while the other 24 are all located on the other main structure.

(B) It belongs to the line $\alpha = 1$, along which the highest-scoring solutions of the coarse grid are concentrated.

(C) The recursive construction used in the model directly yields $\alpha = 1$.

(D) It is located in a region favorable for minimizing the dynamical error.

(E) The highest-scoring point within its local subgrid is $(0.99, 0.51)$, i.e. very close to $(1, \frac{1}{2})$, which is itself the second-highest-scoring configuration.

(F) At the refined-grid level, the exact point $(1, \frac{1}{2})$ lies at the intersection of four neighboring subgrids. Within these local rankings, it is ranked 1st, 2nd, 3rd, and 23rd out of 625 sampled points, respectively.

(G) The value $\beta = \frac{1}{2}$ admits a natural interpretation within the virialized explanation.

These combined observations make $(1, \frac{1}{2})$ a particularly well-supported and physically motivated candidate, despite not corresponding to the absolute maximum of the score.

As a result, it is not possible at this stage to conclusively determine which values of (α, β) correspond to the underlying physical form. Representative examples of the corresponding photometric reconstructions for selected parameter values are provided in Table 3. For the dynamical reconstruction, 169–170 galaxies are resolved across all tested (α, β) values, with relative errors $\sim$ 0.028–0.033 and standard deviations $\sim$ 0.128–0.139, indicating negligible variation between models, in contrast with the photometric results.

Table 3. Photometric correlation analysis for selected (α, β) values.

$\alpha \simeq 1, \quad \beta \geq 2$					
Color	N	r_P	σ_P	ρ_S	σ_S
$(\alpha, \beta) = (1, 3)$					
FUV–NUV	136	0.463	5.68	0.512	6.38
$r - z$	129	0.425	5.02	0.485	5.82
$g - r$	128	0.716	9.51	0.633	8.01
NUV–r	119	0.735	9.52	0.697	8.81
$(\alpha, \beta) = (1, 3.02)$					
FUV–NUV	136	0.462	5.66	0.493	6.09
$r - z$	129	0.444	5.27	0.513	6.21
$g - r$	128	0.729	9.76	0.666	8.58
NUV–r	119	0.740	9.62	0.717	9.16
$(\alpha, \beta) = (0.87, 2.02)$					
FUV–NUV	136	0.472	5.81	0.518	6.46
$r - z$	129	0.434	5.14	0.514	6.22
$g - r$	128	0.758	10.35	0.700	9.19
NUV–r	119	0.764	10.11	0.714	9.12
$\alpha \simeq 1, \quad \beta < 2$					
Color	N	r_P	σ_P	ρ_S	σ_S
$(\alpha, \beta) = (1, 1)$					
FUV–NUV	136	-0.214	2.50	-0.203	2.36
$r - z$	129	0.394	4.63	0.493	5.93
$g - r$	128	0.670	8.66	0.655	8.40
NUV–r	119	0.682	8.53	0.701	8.87
$(\alpha, \beta) = (1, \frac{1}{2})$					
FUV–NUV	136	0.431	5.23	0.485	5.98
$r - z$	129	0.315	3.64	0.438	5.19
$g - r$	128	0.687	8.96	0.683	8.88
NUV–r	119	0.707	8.99	0.684	8.57
$(\alpha, \beta) = (0.99, 0.51)$					
FUV–NUV	136	0.402	4.85	0.521	6.50
$r - z$	129	0.412	4.85	0.504	6.09
$g - r$	128	0.697	9.13	0.681	8.84
NUV–r	119	0.715	9.13	0.707	8.98

5. Discussion

The formulation introduced in this work provides an alternative way to evaluate gravitational binding energy by removing the dependence on arbitrary reference levels. By comparing a distributed configuration to a compact state conserving volume, the resulting quantity can be interpreted as an intrinsic energy associated with the structure of matter.

One of the most notable outcomes of this approach is the relative insignificance of the interaction term $-GmM/d$ in realistic astrophysical configurations. When $d \gg R \gg r$, this term becomes negligible compared to the internal contributions proportional to M^2/R. This suggests that, at large scales, gravitational energy is primarily governed by the internal structure of matter rather than by the spatial separation of its components.

This result should not be interpreted as a contradiction with standard gravitational theory. In classical mechanics, gravitational potential energy is primarily defined within a dynamical framework, through the Lagrangian or Hamiltonian formalism. In this context, the relevant quantity is the energy associated with reversible motion, that is, the work that can be exchanged through changes in the configuration of bodies.

By construction, this approach focuses on conservative interactions and does not aim to describe the energy released during irreversible processes such as inelastic mergers or structural reconfigurations of matter. The conventional expression $-GmM/d$ is therefore well suited for orbital dynamics, but it does not capture the total energy that can be liberated when a system transitions between different structural states.

The formulation proposed in this work addresses this complementary aspect by evaluating the energy difference between configurations that conserve mass and volume but differ in their internal organization. In this sense, it does not replace the classical description, but extends it to account for the energy associated with the assembly or disassembly of gravitationally bound systems.

The invariance properties demonstrated in this work, both under permutations and hierarchical aggregation, further support the interpretation of gravitational binding energy as an intrinsic quantity. These properties ensure that the total energy depends only on the set of constituents and not on the specific assembly path or grouping.

When expressed through the mass–energy equivalence relation $E = mc^2$, the evaluated binding energy corresponds to an effective mass scale. As shown in Table 2, this contribution remains negligible at small scales but grows rapidly for larger systems. At galactic scales, the magnitude of this effective mass becomes comparable to the baryonic mass. This is the regime where the effect is no longer a small correction.

This scaling behavior suggests a possible connection with the mass discrepancy observed in galaxies. However, the extent to which gravitational binding energy alone can account for the full range of observational constraints remains an open question. In particular, beyond the rotation-curve agreement tested here, it remains necessary to assess whether the spatial distribution implied by this energy is consistent with gravitational lensing and large-scale structure formation.

The empirical results are consistent with the hierarchical Newtonian construction. The preference for α close to unity indicates that the binding-energy contributions of the stellar population classes are retained with approximately their natural Newtonian weight. These classes therefore behave as physically meaningful hierarchical subsystems, rather than being absorbed into a purely global homogeneous term.

This also clarifies the role of the global contribution. The class-level term is obtained by aggregating objects of comparable intrinsic density into homogeneous compact subsystems, while the global term describes the subsequent aggregation of these heterogeneous subsystems into a larger volume-conserving configuration. Since these subsystems may have very different intrinsic densities, the global term should not be interpreted as the binding energy of a truly homogeneous solid sphere, but as an effective Newtonian continuum approximation to their mutual aggregation energy. In such a global aggregate, a virial-like factor can reduce the effective contribution relative to the full compact-sphere term, providing a possible interpretation of the empirical preference for $\beta \simeq 1/2$.

This preference should not be interpreted as a definitive selection of the coefficients. The empirical parameter space remains complex and highly structured. The best solutions are not concentrated around a single isolated point, but are distributed along at least two distinct structures in the (α, β) plane. These structures contain several acceptable candidates, including forms close to $(1, \frac{1}{2})$, $(1, 3)$, and $(1, \frac{5}{2})$.

Thus, the empirical results constrain a family of admissible estimators rather than selecting a single final expression. The value $(1, \frac{1}{2})$ remains especially interesting because it has a simple physical interpretation, but the present analysis does not allow one to decide uniquely between the different high-quality candidates.

A natural limitation of the present formulation arises when approaching relativistic regimes. The construction relies on a comparison between configurations that conserve volume and mass, implicitly assuming that the internal structure of matter can be described within a Newtonian framework. However, the construction may formally lead to compact configurations with radii smaller than the Schwarzschild radius. Such configurations do not correspond to physical states within the present framework, as no static configuration can exist in this regime. This indicates that the formulation extrapolates beyond its domain of validity, rather than revealing a physical property of gravitational binding energy.

The relativistic limitation does not invalidate the recursive absorption law itself. It limits the interpretation of the compact reference radius as the radius of a material configuration. The equation may be constructed from Newtonian arguments only while the equivalent compact configuration satisfies $R > R_s$, but once the same function describes the energy absorbed by a black hole for a small amount of external matter, the no-hair property strongly constrains any possible change of functional form.

Indeed, after each absorption event, the final object is again a black hole characterized only by its global parameters. It cannot distinguish whether the absorbed contribution came from one additional small component or from a larger collection of components. Therefore, if the recursive energy-accounting function is valid for the absorption of a small amount of matter by a black hole, the same functional form should remain valid for successive absorptions, unless a new global physical criterion is introduced. The breakdown concerns the interpretation of the intermediate compact material state, not the functional form of the absorbed-energy equation.

The recursive form is consistent with this reasoning. At each step of a sequential absorption process, the

newly absorbed subsystem contributes its own class-level energy, while the global term is updated to the new total mass and effective radius. Once absorbed, these contributions are no longer distinguishable as separate structures, but they remain part of the total mass–energy balance.

Thus, the recursive estimator should not be interpreted as assigning internal structure to a black hole. Rather, it provides an effective accounting of the energy carried by absorbed constituents before they cease to be distinguishable. The black hole erases the observable substructure, but it does not provide a reason for changing the functional dependence of the absorbed energy from one absorption step to the next.

Although the black-hole aggregation argument supports the compatibility of the Newtonian expression with a relativistic mass–energy balance, it is not by itself a relativistic derivation. If a complete analytical derivation in general relativity can be obtained, it may contain additional terms. However, in the weak-field regime relevant to galaxies, such corrections are expected to appear as higher-order contributions, typically suppressed by powers of $1/c^2$, $1/c^4$, and so on. The observational results obtained indicate that the Newtonian terms already capture the dominant contribution. A discrepancy of this magnitude is unlikely to be explained by small higher-order relativistic corrections alone, whereas the Newtonian terms identified here already appear at the required scale.

The empirical search for the correct functional form of energy is not new in physics. The concept of energy itself was not fixed from the beginning of mechanics, but emerged through a long process of clarification in which different physical quantities had to be distinguished. In the early development of mechanics, the correct dependence of kinetic energy on velocity was debated between proportionality to mv and mv^2. The experimental and theoretical work of Émilie du Châtelet, published in 1740, played an important role in supporting the quadratic dependence, which was subsequently incorporated into the analytical formulation of mechanics by d'Alembert in 1743, leading to the modern expression $\frac{1}{2}mv^2$. This historical example illustrates both the evolving nature of the energy concept and the role of empirical constraints in identifying the correct functional form when the underlying theoretical structure is not yet fully established.

The present work follows a similar logic at a different level. The proposed estimator is not selected solely from dimensional arguments or formal simplicity, but is tested by allowing the relative weights of its two terms to vary. The purpose of the empirical exploration is therefore to determine whether the data favor the relative weights predicted by the hierarchical Newtonian construction, or whether deviations from these weights indicate that the formulation is incomplete.

The results support the view that the functional form is not arbitrary. The preferred region, especially the vicinity of $(\alpha, \beta) = (1, \frac{1}{2})$, is supported by the recursive interpretation of the class-level term, by the possible virial interpretation of the global heterogeneous aggregate, and by the observational reconstruction tests. Related structures appear in both dynamical and photometric maps constrains the admissible forms of the energy and indicates that the parameter dependence is tied to the reconstructed stellar-population structure rather than to a purely numerical artifact.

6. Conclusion

This work developed a hierarchical Newtonian evaluation of gravitational binding energy in galactic systems. The central result is that the relevant energy is not exhausted by a single compact-sphere term. A correct accounting retains the binding energy stored in homogeneous stellar population classes and adds the global aggregation energy associated with combining these compact subsystems into a larger volume-conserving configuration.

This naturally leads to a two-term estimator. The class-level contribution has a direct recursive interpretation and favors $\alpha \simeq 1$, while the global heterogeneous aggregation term may admit an effective virial reduction, providing a possible interpretation of $\beta \simeq 1/2$. The empirical exploration of the (α, β) parameter space supports this structure, but does not select a unique analytical form. Instead, the parameter-space landscape contains several high-quality regions, including candidates near $(1, \frac{5}{2})$ and $(1, \frac{1}{2})$.

The observational tests provide an independent constraint on the formulation. Stellar populations reconstructed from dynamical information alone produce statistically significant correlations with GALEX and SDSS colors. This shows that the reconstruction does not merely reproduce an effective dark mass numerically, but also captures information related to stellar population structure.

The transition to the relativistic regime can be approached through a limiting absorption argument. The Newtonian compact-reference construction is valid only while the equivalent compact radius remains outside the Schwarzschild limit. Beyond it, the compact material state is no longer physically meaningful, but the same energy-accounting function can still be followed through sequential absorption by a black hole.

This provides a natural bridge between the Newtonian construction and a relativistic mass–energy bal-

ance. If the function correctly describes the energy carried by a subsystem before absorption, the no-hair property implies that the final black hole cannot retain information about the internal decomposition of the absorbed matter. The absorbed class-level contributions therefore cease to be observable as separate structures, but they remain part of the total mass–energy budget. In this sense, black-hole absorption allows the recursive energy form to be extended beyond the material compact-sphere regime without requiring a full general-relativistic reconstruction of the intermediate compact state.

Taken together, these results support gravitational binding energy, evaluated hierarchically, as a plausible and testable contribution to the effective dark mass inferred from galactic dynamics. Future observational tests should examine whether the same energy function can be extended beyond rotation curves, including gravitational lensing, galaxy groups, galaxy clusters, cluster mergers, large-scale structure, and the influence of the turnaround distance on the inferred effective mass.

The present work does not establish a unique final form for gravitational binding energy in astrophysical systems, but it substantially narrows the range of admissible forms. The combined mathematical, dynamical, and photometric evidence points toward a hierarchical recursive estimator in which stellar population classes retain their own binding-energy contributions, while the global term accounts for their subsequent aggregation into the final heterogeneous configuration with an effective virial factor of one half.

Software Availability

The C++ program used to perform all numerical calculations and generate the corresponding graphs are freely available at `dark-mass-generator.sourceforge.io` or at `doi.org/10.6084/m9.figshare.31894372`.

Declarations

Funding — This research received no specific grant from any funding agency in the public, commercial, or not-for-profit sectors.
Competing interests — The author declares no competing interests.
Ethics approval / Consent — Not applicable.
Data and materials availability — See "Software availability".
Author contribution – N.P. conceived the study, performed the analysis, and wrote the manuscript.

References

Bartelmann, M. 2010, Classical and Quantum Gravity, 27, 233001

Brillouin, L. 1965, Proceedings of the National Academy of Sciences of the United States of America, 53

Clowe, D., Bradač, M., Gonzalez, A. H., *et al*. 2006, The Astrophysical Journal Letters, 648, L109

Courteau, S., *et al*. 2014, Reviews of Modern Physics, 86, 47

Deur, A. 2021, European Physical Journal C, 81, 213

—. 2022, Classical and Quantum Gravity, 39, 135003

Deur, A., Sargent, C., & Terzic, B. 2020, The Astrophysical Journal, 896, 94

Hawking, S. W. 1968, Journal of Mathematical Physics, 9, 598

Hayward, S. A. 1996, Physical Review D, 53, 1938

Landau, L. D., & Lifshitz, E. M. 1976, Course of Theoretical Physics, Vol. 1, Mechanics, 3rd edn. (Oxford: Butterworth-Heinemann)

Lelli, F., McGaugh, S. S., & Schombert, J. M. 2016, The Astronomical Journal, 152, 157

Martin, D. C., *et al*. 2005, The Astrophysical Journal Letters, 619, L1

MICROSCOPE Collaboration. 2022, Phys. Rev. Lett., 129, 121102

Misner, C. W., & Sharp, D. H. 1964, Physical Review, 136, B571

Persic, M., Salucci, P., & Stel, F. 1996, Monthly Notices of the Royal Astronomical Society, 281, 27

Poupart, N. 2014, General Science Journal, available online at General Science Journal

—. 2025, Dark Mass is Potential Energy, preprint, doi:10.6084/m9.figshare.30543407

—. 2026, Stellar Population Ordering from Galactic Dynamics, preprint, doi:10.6084/m9.figshare.31175302

Rubin, V. C., Ford, W. Kent, J., & Thonnard, N. 1980, The Astrophysical Journal, 238, 471

York, D. G., *et al*. 2000, The Astronomical Journal, 120, 1579